MOLECULAR DYNAMICS OF *TRANS-CIS* ISOMERIZATION IN BATHORHODOPSIN

ROBERT R. BIRGE AND LYNN M. HUBBARD, *Department of Chemistry, University of California, Riverside, California 92521*

ABSTRACT Semiempirical molecular dynamics procedures are used to theoretically investigate the trajectories and quantum yields of the rhodopsin → bathorhodopsin and bathorhodopsin → rhodopsin photoisomerizations. The calculations are based on the semiclassical trajectory formalism and rhodopsin binding site model proposed by Birge and Hubbard (1980. *J. Am. Chem. Soc.* 102: 2195–2205). The rhodopsin → bathorhodopsin photoisomerization is predicted to occur in ~2.2 ps with a quantum yield of 0.62 in reasonable agreement with experiment (<6 ps, ϕ = 0.67). The bathorhodopsin → rhodopsin photoisomerization is predicted to occur in ~1.8 ps with a quantum yield of 0.48. The latter number is in good agreement with the observed quantum yield for cattle bathorhodopsin (ϕ = 0.5) but in poor agreement with the observed value for squid bathorhodopsin (ϕ = 0.36). Our calculations suggest that the observed photochemical preference of the chromophore in cattle bathorhodopsin to isomerize to form rhodopsin (ϕ = 0.5), instead of isorhodopsin (ϕ = 0.054), is associated with a significant out-of-plane distortion (9–17°) of the 11,12-*trans* dihedral angle in the batho chromophore.

INTRODUCTION

Yoshizawa and Wald's observation in 1963 (1) of a photochemical equilibrium among rhodopsin, bathorhodopsin, and isorhodopsin provided the first experimental evidence that the chromophore in bathorhodopsin has an all-*trans* or *"transoid"* conformation. This assignment follows from the characterization of the chromophore geometries in rhodopsin and isorhodopsin as involving different double-bond isomers (2).

$$\underset{(11\text{-}cis)}{\text{rhodopsin}} \underset{h\nu}{\overset{h\nu}{\rightleftharpoons}} \text{bathorhodopsin} \underset{h\nu}{\overset{h\nu}{\rightleftharpoons}} \underset{(9\text{-}cis)}{\text{isorhodopsin}}$$

The all-*trans* assignment for bathorhodopsin was generally accepted until 1972 when Busch, et al. (3), spectroscopically observed that bathorhodopsin is formed in <6 ps. This time period was considered by many to be too short to accommodate a one-bond *cis-trans* isomerization, and a number of alternative mechanisms were proposed (3–9). The observation of a deuterium isotope effect on the rhodopsin-to-bathorhodopsin rate (5) added additional weight to those models involving proton translocation (3–8). However, none of the alternative mechanisms could adequately account for the above mentioned photoequilibrium. Furthermore, molecular dynamics calculations demonstrate that photochemical isomerization in

---

Dr. Hubbard's present address is the Department of Chemistry, University of California, Berkeley, California 94720.

rhodopsin may be much faster than previously suspected (10, 11). In particular, recent calculations predict that a one-bond photochemical 11-*cis* to 11-*trans* isomerization can occur with high quantum efficiency ($\phi_{calc} \simeq 0.6$) in ~2 ps (11).

The molecular dynamics calculations (10, 11); resonance Raman studies of chromophore analogs in bathorhodopsin (12); bleaching studies using chromophore analogs (13); the observed photochemical equilibrium among rhodopsin, bathorhodopsin, and isorhodopsin (1); and other recent studies (14–21) combine to form overwhelming evidence that the chromophore in bathorhodopsin has a distorted all-*trans* conformation. What remains to be fully explained is the source of the deuterium isotope effect, but a number of reasonable hypotheses have been proposed that accommodate isomerization (2, 15, 20).

The present theoretical investigation of the molecular dynamics of the photochemical transformation of bathorhodopsin to rhodopsin was prompted by the recent quantum-yield studies of Suzuki and Callender (22). These investigators measured the quantum yields for transformation among rhodopsin, bathorhodopsin, and isorhodopsin in both cattle (vertebrate) and squid (invertebrate) pigment systems. Their experimental results are summarized below:

$$\text{cattle: rhodopsin} \underset{0.50}{\overset{0.67}{\rightleftharpoons}} \text{bathorhodopsin} \underset{0.10}{\overset{0.054}{\rightleftharpoons}} \text{isorhodopsin}$$

$$\text{squid: rhodopsin} \underset{0.36}{\overset{0.67}{\rightleftharpoons}} \text{bathorhodopsin} \underset{0.16}{\overset{0.24}{\rightleftharpoons}} \text{isorhodopsin,}$$

where the photochemical quantum yields are shown above, or below the appropriate arrows. (The rhodopsin → bathorhodopsin quantum yield is from reference 23.) It is interesting to note the marked difference between the photochemistry of cattle vs. squid bathorhodopsin. This observation indicates that significant differences exist in the binding sites of cattle and squid pigments and that the chromophore in cattle bathorhodopsin may exhibit significant out-of-plane distortion in the 11,12 dihedral angle (see below). Of equal importance to the present study is the observation that the quantum yields for cattle rhodopsin and bathorhodopsin photochemistry add up to >1, and differ in magnitude by 0.17. The fact that the quantum yields sum to ~1.2 indicates isomerization must proceed from a nonequilibrated activated complex. The fact that the quantum yield is ~30% larger in the "forward" direction (0.67) than in the "reverse" direction (0.5) indicates a significant difference in the forward and reverse isomerization trajectories.

The molecular dynamics calculations presented in this paper are an extension of the calculations on the 11-*cis* to *trans* isomerization of the chromophore in rhodopsin given in reference 11. Our previous treatment investigated the trajectories associated with the potential surface of the first excited $\pi\pi^*$ singlet state of (A) the free chromophore and (B) the chromophore bound to the lysine residue in the rhodopsin binding site. An initial treatment of the trajectories associated with potential surface (B) modified by the inclusion of a counterion was also presented. We now extend the latter model to investigate the molecular dynamics of the *trans* to 11-*cis* isomerization associated with the bathorhodopsin to rhodopsin photochemical transformation. We also present a detailed examination of the isomerization trajectories and quantum yields for the *cis* → *trans* isomerization of rhodopsin to afford a comparison

between the photochemical behavior of rhodopsin and bathorhodopsin. Our mathematical procedures and basic assumptions are identical to those described in Reference 11, and the trajectory analyses yield the following calculated quantum yields: (*a*) rhodopsin → bathorhodopsin ($\phi_{calc} = 0.62$ [obsvd = 0.67]) (*b*) bathorhodopsin → rhodopsin ($\phi_{calc} = 0.48$ [obsvd = 0.5]). The good agreement with experiment indicates that our simple model for the rhodopsin binding site has merit. Our trajectory calculations therefore provide new insights into the primary photochemical event in the bleaching cycle of vertebrate rhodopsin.

THEORETICAL BACKGROUND

Potential Surfaces for Isomerization

The potential surfaces for the 11-12 dihedral angle in the ground and first excited singlet states of the chromophore in rhodopsin are taken from Birge and Hubbard (11) and are shown in Fig. 1. These surfaces were calculated using a combination of INDO-CISD molecular orbital theory (conformational energy of the retinyl polyene) and consistent force field procedures (conformational energy of the lysine residue). The INDO-CISD calculations include high levels of both single- and double-excitation configuration interaction (CI). Previous calculations have demonstrated the importance of including double CI in calculations on the spectroscopic properties of the visual chromophores (24–27). The reader is referred to Reference 11 for a detailed discussion of the mathematical details.

The principal binding site assumptions that were used in constructing the potential surfaces shown in Fig. 1 are summarized briefly. (*a*) The retinal chromophore is covalently bound to the opsin active site via a protonated Schiff-base linkage to a lysine residue of the protein (see Fig. 2). (*b*) The β-ionylidene ring is trapped in a hydrophobic cleft. During the isomerization, no atom of the β-ionylidene ring can move by >0.05 Å and the center of mass must remain fixed. Recent binding studies suggest that the ring binding site may be quite "lenient" (28), and therefore the above restriction on β-ionylidene motion may be too severe. As discussed below, however, our goal is to err in the direction of overestimating photoisomerization time and the above assumption is consistent with this objective. (*c*) The photochemical isomerization from the 11-*cis* to 11-*trans* conformation is accomplished entirely as one-bond rotation about the 11,12 bond. All other internal degrees of freedon of the chromophore are fixed at the original conformation of the chromophore (6-s-*cis* [45], 12-s-*trans*). (*d*) The first four carbon atoms of the hydrocarbon portion of the lysine residue, and the hydrogens that are bonded to these carbon atoms, are

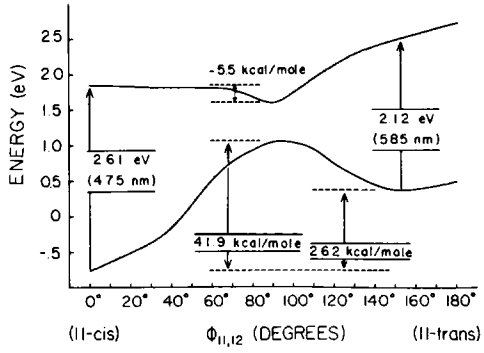

FIGURE 1 Potential energy surfaces for isomerization about the C_{11}—C_{12} bond in the ground state and first excited $\pi\pi^*$ singlet state of the protonated Schiff-base chromophore in rhodopsin. The polyene portion of the potential energy surface was calculated using INDO-CISD molecular orbital theory including ~130 single and ~350 double excitations. The lysine portion of the potential surface was adiabatically mapped using consistent force field procedures. A single counterion was included in the active site (see Fig. 2). A full discussion of the calculational details may be found in reference 11.

allowed to seek their minimal energy conformation during the isomerization process. No other distortions of the protein are allowed. (*e*) A single counterion consisting of the carboxylate group of a glutamic acid residue is placed near the C_{15}=N group as shown in Fig. 2. The counterion is held fixed in space during isomerization and the electrostatic stabilization lost due to charge separation is not corrected for protein dielectric relaxation. These assumptions will tend to overestimate the contribution of the decrease in electrostatic stabilization to the calculated bathochromic shift. As can be seen by reference to Fig. 1, the calculated bathochromic shift is, in fact, overestimated ($\Delta\lambda_{calc}$ = 110 nm, $\Delta\lambda_{obsvd}$ = 43 nm [540 − 497 nm]).

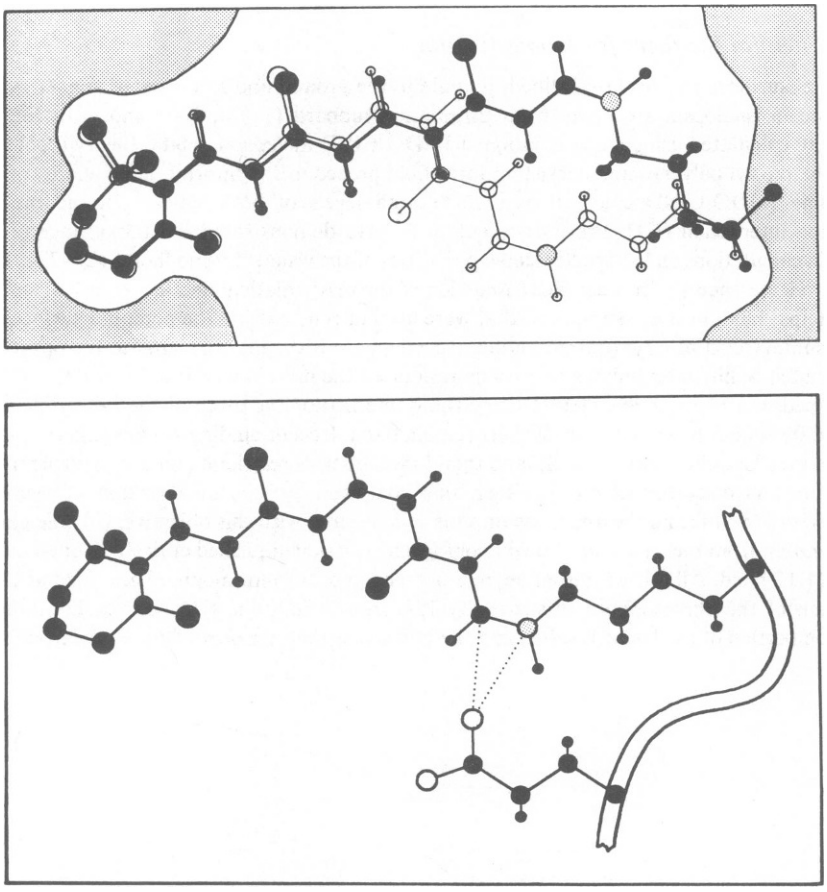

FIGURE 2 Our simplified model of the active site of rhodopsin. The top figure shows the conformation of the chromophore and the hydrocarbon residue of lysine in rhodopsin (atoms represented by open circles) and bathorhodopsin (atoms represented by solid circles). The protonated Schiff base nitrogen is indicated with a shaded circle and the hydrogens on the methyl groups are not shown. The lysine residue in bathorhodopsin is deformed out of the plane and this conformational distortion contributes ~15 kcal/mol to the differential potential energy of bathorhodopsin relative to rhodopsin. The *cis-trans* isomerization is accomplished without significantly disturbing the β-ionylidene ring. The bottom figure shows the location of the counterion in rhodopsin. The counterion consists of the carboxylate group of a glutamic acid residue. One of the oxygen atoms of the carboxylate group is placed 3 Å (dotted lines) from the C_{15} carbon and the N_{16} imino nitrogen atoms. The ribbon connecting the lysine and glutamic acid residues is to schematically indicate that both residues are attached to the same protein backbone.

While the above assumptions are for the most part hypothetical, the resulting potential surfaces (Fig. 1) agree reasonably well with the available experimental data. A comparison of various observed parameters with corresponding values that were calculated based on the potential surfaces of Fig. 1 indicates that all of the spectroscopic and thermodynamic trends are correctly predicted. In particular, the calculated increases in λ_{max} and oscillator strength in going from rhodopsin to bathorhodopsin are in reasonable agreement with experiment (λ_{max}[rhod] = 475 nm [498 obsvd], f[rhod] = 0.87 [0.8 obsvd], λ_{max}[batho] = 585 nm [540 obsvd], f[batho] = 0.98 [0.9 obsvd]). The potential energy difference between bathorhodopsin and rhodopsin is calculated to be 26 kcal/mol (Fig. 1) which is ~9 kcal/mol too small based on recent calorimetric measurements (29). Although this difference is significant, our underestimation of the energy of bathorhodopsin (and therefore the steepness of the excited-state potential surface in the $\phi_{11,12}$ 90–180° region) is not a significant source of error in terms of the calculated isomerization times or quantum yields (see below).

Trajectory and Transition Probability Formalisms

The semiempirical molecular dynamics procedures used for the present investigation of isomerization trajectories are based on the semiclassical formalism of Birge and Hubbard (11). The formalism places restraints on the energy available to the torsional motion by limiting the sources of the torsional kinetic energy to that which is provided by the potential surface. Accordingly, excess vibrational energy is prevented from partitioning into the torsional kinetic energy. In contrast, an efficient pathway is provided for transfer of torsional kinetic energy into "nonproductive" vibrational modes based on a vibrational continuum approximation given by:

$$\left(\frac{\Delta E_{kin}}{\Delta t}\right)_{t=\tau} = -C_m E_{kin}^2(\tau) \qquad (E_{kin} > h\nu_l) \tag{1}$$

where $(\Delta E_{kin}/\Delta t)_{t=\tau}$ is the rate of loss of torsional kinetic energy at trajectory time τ, $E_{kin}(\tau)$ is the torsional kinetic energy at $t = \tau$, and $h\nu_l$ is the energy of the lowest vibrational mode capable of scavenging torsional kinetic energy (see below). C_m is a semiempirical constant which is equal to the vibrational coupling efficiency.

The trajectory calculations presented here are designed to err in the direction of overestimating trajectory times. Accordingly, we have chosen a relatively large value for C_m of $1/2(h^{-1})$ and a relatively small $h\nu_l$ of 50 cm^{-1} (11). We are confident that these parameters will overestimate vibrational scavenging of the torsional kinetic energy but calculations including all degrees of freedom would be required to test this point. Furthermore, the possibility of reverse coupling whereby vibrational energy is transferred back into the torsional degree of freedom is ignored in our trajectory calculation.

The experimental observation of a wavelength-independent quantum yield for rhodopsin isomerization indicates that excess vibrational energy of the chromophore (E_{vib}) is rapidly transferred to the protein matrix. We simulate this process using a density of states approximation,

$$\left(\frac{\Delta E_{vib}}{\Delta t}\right)_{t=\tau} = -\left|\frac{\Delta E_{vib}}{\Delta t}\right|_{ave}\{1 - e^{-\rho[E_{vib}(\tau)-kT]}\} - \left(\frac{\Delta E_{kin}}{\Delta t}\right)_{t=\tau}, \tag{2}$$

where $(\Delta E_{vib}/\Delta t)_{t=\tau}$ is the rate of vibrational relaxation at trajectory time τ, $|\Delta E_{vib}/\Delta t|_{ave}$ is the absolute (exponential) average vibrational relaxation rate, ρ is the density of states factor, E_{vib} (τ) is the vibrational energy at trajectory time τ, k is the Boltzmann constant, T is the temperature (300°K) and $(\Delta E_{kin}/\Delta t)_{t=\tau}$ is calculated using Eq. 1. Eq. 2 indicates that vibrational energy is lost through relaxation processes but gained through transfer of torsional kinetic energy into the vibrational manifold. The salient parameters were adjusted to produce a wavelength-independent quantum yield for isomerization yielding $|\Delta E_{vib}/\Delta t|_{ave}$ = 2 eV/ps and ρ = 1 eV^{-1} (11).

A theoretical prediction of quantum yields for isomerization based on our trajectory analysis can be obtained by calculating the probability of crossing into the ground state $a_0^2(\tau)$, as a function of trajectory time, τ. A time-dependent quantum mechanical treatment (10, 11, 30, 31) yields,

$$a_0^2(\tau) = \left\{ \int_0^\tau \left[\left\langle \psi_0 \left| \frac{\partial \psi_1}{\partial t} \right\rangle a_1(t) \exp\left(-\frac{i}{\hbar} \int_0^t \Delta E_{10} dt' \right) \right] dt \right\}^2 \tag{3}$$

where ψ_0 and ψ_1 are the electronic wavefunctions of the ground and excited state and ΔE_{10} ($= E^* - E^\circ$) is the time-dependent potential energy difference between the excited state and the ground state. Unfortunately, solution of the nonadiabatic coupling function $\langle \psi_0 | \partial \psi_1 / \partial t \rangle$ is not possible within the confines of our semiempirical trajectory formalism without the introduction of serious *ad hoc* assumptions. Accordingly, we calculate $a_0^2(\tau)$ using a semiclassical solution to Eq. 3,

$$a_0^2(\tau) = \exp - \left\{ \left(\frac{4\Delta W(\tau)}{3\hbar} \right) \left[\frac{2\Delta W(\tau)}{(\partial^2 \Delta E_{10}/\partial t^2)_{t=\tau}} \right]^{1/2} \right\} \tag{4}$$

where $\Delta W(\tau)$ is the adiabatic potential energy difference between the ground and excited state adjusted with respect to the Born-Oppenheimer local minimum (11):

$$\Delta W(\tau) = \Delta E_{10}(\tau) - \Delta E_{10}(\ell m) + \tfrac{1}{4} E_{\text{vib}}(\tau) \tag{5}$$

$\Delta E_{10}(\ell m)$ is the difference in the excited-state and ground-state potential energy surfaces at their minimum engery separation ($\phi_{11,12} = 90°$). The purpose of using $\Delta W(\tau)$ rather than $\Delta E_{10}(\tau)$ in our calculation of ground state crossing probabilities is to semiempirically introduce coordinate relaxation processes in our model. Note that the potential surfaces shown in Fig. 1 were calculated assuming only one degree of freedom for the polyene coordinates ($\phi_{11,12}$) and all other internal degrees of freedom of the polyene were held fixed at the original (ground-state) values. It is reasonable to assume, however, that equilibration of the other degrees of freedom of the polyene residue will occur after excitation and that this process will be roughly proportional in time to the rate of vibrational energy loss to the protein matrix. In other words, as the polyene distributes the excess vibrational energy to the protein, the polyene simultaneously relaxes to a minimum excited-state energy so that the difference in energy between the ground- and excited-state potential surfaces decreases. Eq. 5 naively predicts that the S_1 and S_0 surfaces will converge when $E_{\text{vib}} = 0$, but in actuality the vibrational energy is calculated to decrease to no less than 0.07 eV (~560 cm^{-1}) above the zero-point energy before complete internal conversion to the ground state. Recent calculations on the first excited singlet state energy of the protonated Schiff base of retinal using a partial gradient minimization of the excited state geometry predict that the S_1 and S_0 surfaces approach an energy difference of ~0.1 eV (R. R. Birge, B. M. Pierce, and L. M. Hubbard, unpublished results). Accordingly, the assumptions inherent in the application of Eq. 5 are justified. However, our assumption that the S_0 and S_1 potential surface separation is proportional to $1/4(E_{\text{vib}})$ is purely empirical and is based on the expectation that coordinate relaxation is roughly four times slower than radiationless decay in the present system.

The calculations reported in this paper were carried out using trajectory increments of 10^{-15} s. At each time increment, the classical (Newtonian) equations of motion are solved in double precision (16 significant digits) using five point Lagrangian interpolation formulae to calculate the energy of the potential surface at $\phi_{11,12}(\tau)$ and the gradients of force and the temporal derivatives that appear in Eqs. 1, 2, and 4 (see Appendix). Test calculations were performed using smaller (10^{-16} s) and larger (10^{-14} s) increments in time to determine the effect of changes in this arbitrary parameter on the calculated properties. Calculations using increments of 10^{-15} and 10^{-16} s produced results that agreed to within four significant digits. Although an increment of 10^{-14} s appears to be adequate for calculations of trajectory times, this interval is too coarse to accurately calculate $a_0^2(\tau)$ because of calculational error associated with evaluation of the $\partial^2 \Delta E_{10}/\partial t^2$ term in Eq. 4.

RESULTS AND DISCUSSION

Isomerization trajectories after excitation into the first excited singlet states of rhodopsin and bathorhodopsin are shown in Figs. 3 and 4. The molecules are promoted into the excited state

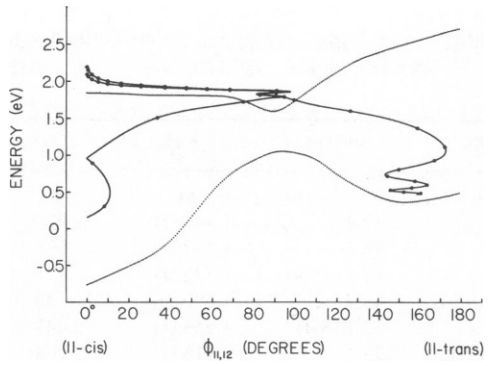

FIGURE 3

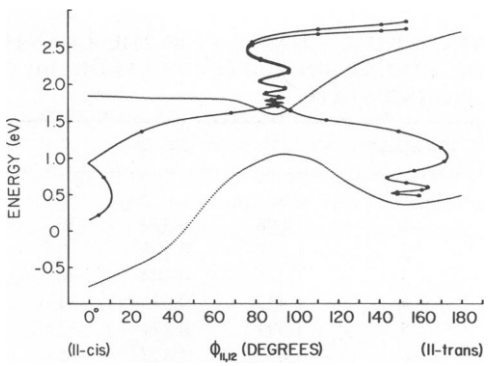

FIGURE 4

FIGURE 3 Molecular dynamics of *cis-trans* isomerization in rhodopsin based on the potential surfaces of Fig. 1. The excited-state trajectory enters the activated complex in ~1.1 ps and oscillates with an average frequency of torsional motion of $\sim 4.5 \times 10^{12}$ Hz (~ 150 cm^{-1}). The lower left trajectory leads to the starting geometry (rhodopsin) in 1.8 ps; the lower right trajectory leads to isomerized product (bathorhodopsin) in 2.2 ps. These trajectories are shown in passes 3 and 4 in Table I, and along with trajectories 1 and 2 are responsible for depleting the S_1 ($\pi\pi^*$) surface leaving a fraction of less than e^{-1} (0.37) of the molecules in the excited state. The solid circles indicate trajectory increments of 0.1 ps. The two different excited-state trajectories differ in excitation energy by 0.1 eV but coallesce before reaching the activated complex to produce wavelength-independent isomerization trajectories and quantum yields. The lower left trajectory actually continues beyond the range of the horizontal axis to $\phi_{11,12} = -11°$ but is shown reflected back towards positive dihedral angles for convenience.

FIGURE 4 Molecular dynamics of *trans-cis* isomerization in bathorhodopsin based on the potential surfaces of Fig. 1. The excited-state trajectory enters the activated complex in ~0.3 ps and oscillates with an average frequency of torsional motion of $\sim 4.6 \times 10^{12}$ Hz (~ 155 cm^{-1}). The lower left trajectory leads to isomerized product (rhodopsin) in 1.8 ps; the lower right trajectory leads to the starting geometry (bathorhodopsin) in 2.2 ps. These trajectories are shown in passes 10 and 11 in Table II, and along with trajectories 1–9 are responsible for depleting the S_1 ($\pi\pi^*$) surface leaving a fraction of less than e^{-1} (0.37) of the molecules in the excited state. The comments in the last three sentences of the caption to Fig. 3 also apply to Fig. 4.

from a rest position with an excess vibrational energy (E_{vib}) of 0.25 or 0.35 eV. This excess energy is rapidly dissipated so that the molecules enter the potential well at $\phi_{11,12} = 90°$ with virtually identical vibrational energy regardless of initial energy. Because the dynamics of internal conversion into the ground state are associated entirely with the torsional behavior in the potential well, the calculated quantum yields of isomerization are very insensitive to the amount of initial excess vibrational energy. The calculations therefore reproduce the experimentally observed wavelength independence of the quantum yields. It should be noted that we adjusted Eq. 2 to produce this wavelength independence so the above observations are not indicative of successful theoretical prediction but rather successful parametrization.

An important limitation of our theoretical treatment of bathorhodopsin is due to our neglect of the 9,10 torsional coordinate. Accordingly, excitation of bathorhodopsin is falsely predicted to produce only rhodopsin (11-*cis*) or bathorhodopsin (11-*trans*) but no isorhodopsin (9-*cis*). This limitation is not a serious defect in simulating cattle pigment photochemistry because the observed quantum yield of formation of isorhodopsin from bathorhodopsin is only 0.054. Consequently, neglect of the 9,10 coordinate does not introduce significant error in simulating

TABLE I

STATISTICAL ANALYSIS OF THE QUANTUM YIELD FOR *CIS* → *TRANS* ISOMERIZATION OF RHODOPSIN BASED ON PROBABILITIES OF TRAJECTORY SPLITTING INTO THE GROUND STATE

Pass No.*	τ‡	$a_0^2(\tau)$§	S_1‖	S_0^{cis}¶	S_0^{trans}**	τ_0^t§§	τ_0^c‖‖
	ps		%	%	%	*ps*	*ps*
1	1.098	0.333	66.7	0.0	33.3	1.447 (*t*)	1.921
2	1.200	0.238	50.8	15.9	33.3	1.447 (*c*)	1.596
3	1.345	0.204	40.5	15.9	43.7 (10.4)	1.722 (*t*)	2.191
4	1.435	0.235	31.0	25.4 (9.5)	43.7	1.690 (*c*)	1.839
5	1.571	0.271	22.6	25.4	52.1 (8.4)	1.959 (*t*)	2.442
6	1.655	0.317	15.4	32.5 (7.1)	52.1	1.915 (*c*)	2.064
7	1.788	0.370	9.7	32.5	57.8 (5.7)	2.200 (*t*)	2.665
8	1.869	0.415	5.7	36.5 (4.0)	57.8	2.133 (*c*)	2.282
9	2.002	0.466	3.0	36.5	60.4 (2.6)	nc¶¶	nc
10	2.079	0.503	1.5	38.1 (1.6)	60.4	nc	nc
11	2.212	0.545	0.6	38.1	61.3 (0.9)	nc	nc
12	2.287	0.573	0.3	38.4 (0.3)	61.3	nc	nc
13	2.420	0.605	0.1	38.4	61.5 (0.2)	nc	nc
14	2.493	0.625	0.0	38.5 (0.1)	61.5	nc	nc

*Trajectory pass through the 90° dihedral angle of the 11, 12 bond. Trajectory passes 3 and 4 are shown in Fig. 3.
‡Trajectory time.
§Probability of crossing into the ground state at τ.
‖Percentage of molecules remaining in the excited state after trajectory splitting.
¶Percentage of molecules that will equilibriate to form unisomerized (11-*cis*) conformation (Δ% for individual trajectory in parentheses).
**Percentage of molecules that will equilibriate to form isomerized (11-*trans*) conformation (Δ% for individual trajectory in parentheses).
§§Total trajectory time until molecule reaches "edge" of its ground state trajectory with excess vibrational energy. The resulting geometry is indicated in parentheses (*t*, 11-*transoid*; *c*, 11-*cis*).
‖‖Total trajectory time for molecule to reach "relaxed" ground state (see text).
¶¶nc, not calculated.

cattle rhodopsin photochemistry. However, our calculations are clearly less relevant to squid pigment photochemistry.

Isomerization Time

Figs. 3 and 4 show only two of the many trajectories that are associated with depopulation of the excited-state manifold and repopulation of the ground state. Analyses of individual trajectories for the photoisomerization of rhodopsin and bathorhodopsin are presented in Tables I and II.[1] We define the "isomerization time" as the time required to repopulate the "relaxed" ground state leaving a fraction of less than e^{-1} (0.37) molecules in the excited state. Table I indicates that only four torsional oscillations (in the activated complex) are necessary to return >63% ($1 - e^{-1}$) of the excited molecules to the ground state during 11-*cis* to 11-*trans* isomerization of rhodopsin. The isomerization time is calculated to be 2.19 ps. In contrast, 11 torsional oscillations are necessary to return >63% of the excited molecules to the

[1]Note that the calculations presented in Table I differ only slightly from those presented in Table II of reference 11. The latter calculations did not include the effects of a counterion on the potential surface and predict a slightly smaller quantum yield of isomerization.

TABLE II

STATISTICAL ANALYSIS OF THE QUANTUM YIELD FOR *TRANS* → *CIS* ISOMERIZATION OF BATHORHODOPSIN BASED ON PROBABILITIES OF TRAJECTORY SPLITTING INTO THE GROUND STATE

Pass No.*	τ‡	$a_0^2(\tau)$§	S_1‖	S_0^{cis}¶	S_0^{trans}**	τ_0^*‡‡	τ_0'§§
	ps		%	%	%	*ps*	*ps*
3	0.533	0.001	99.9	0.1	0.0	nc‖‖	nc
4	0.672	0.004	99.5	0.1	0.4	nc	nc
5	0.763	0.013	98.2	1.3 (1.2)	0.4	nc	nc
6	0.896	0.037	94.6	1.3	4.1 (3.7)	1.296 (*t*)	1.759
7	0.981	0.068	88.1	7.8 (6.5)	4.1	1.241 (*c*)	1.390
8	1.112	0.127	76.9	7.8	15.3 (11.2)	1.529 (*t*)	2.000
9	1.194	0.177	63.3	21.4 (13.6)	15.3	1.458 (*c*)	1.607
10	1.324	0.256	47.1	21.4	31.4 (16.1)	1.747 (*t*)	2.231
11	1.403	0.310	32.5	36.0 (14.6)	31.4	1.670 (*c*)	1.818
12	1.534	0.385	20.0	36.0	44.0 (12.6)	1.981 (*t*)	2.468
13	1.610	0.431	11.4	44.7 (8.7)	44.0	1.879 (*t*)	2.028
14	1.742	0.492	5.8	44.7	49.6 (5.6)	nc	nc
15	1.815	0.526	2.7	47.7 (3.0)	49.6	nc	nc
16	1.948	0.570	1.2	47.7	51.1 (1.5)	nc	nc
17	2.019	0.594	0.5	48.4 (0.7)	51.1	nc	nc
18	2.153	0.624	0.2	48.4	51.4 (0.3)	nc	nc

*Trajectory pass through the 90° dihedral angle of the 11, 12 bond. Trajectory passes 10 and 11 are shown in Fig. 4.
‡Trajectory time.
§Probability of crossing into the ground state at τ.
‖Percentage of molecules remaining in the excited state after trajectory splitting.
¶Percentage of molecules that will equilibriate to form isomerized (11-*cis*) conformation (Δ% for individual trajectory in parentheses).
**Percentage of molecules that will equilibriate to form unisomerized (11-*trans*) conformation (Δ% for individual trajectory in parentheses).
‡‡Total trajectory time until molecule reaches "edge" of its ground state trajectory with excess vibrational energy. The resulting geometry is indicated in parentheses (*t*, 11-*transoid; c*, 11-*cis*).
§§Total trajectory time for molecule to reach "relaxed" ground state (see text).
‖‖nc, not calculated.

ground state during 11-*trans* to 11-*cis* isomerization of bathorhodopsin (Table II). The reason for this significant difference is analyzed below, and it is surprising to observe that the net isomerization time is calculated to decrease slightly to 1.82 ps. In summary, therefore, our calculations predict that isomerization of rhodopsin and bathorhodopsin occurs in ~2 ps after excitation.

Quantum Yields of Isomerization

The quantum yield of isomerization is calculated by statistically analyzing the probabilities of trajectory splitting into the ground state manifold. As shown in Figs. 5 and 6, graphs of the probability of crossing into the ground state as a function of time display sharply peaked maxima. These maxima correspond to trajectory passes through the $\phi_{11,12} = 90°$ dihedral angle coordinate along the potential surfaces of Figs. 3 and 4. The difference in the ground- and excited-state potential energy is minimized at $\phi_{11,12} = 90°$ (ΔW is small) and the surface curvature and velocity are maximized at $\phi_{11,12} = 90°$ ($\partial^2 E_{10}/\partial t^2$ is maximum, see Figs. 5 and 6). Evaluation of Eq. 4 indicates that small ΔW and large $\partial^2 E_{10}/\partial t^2$ produce a maximum

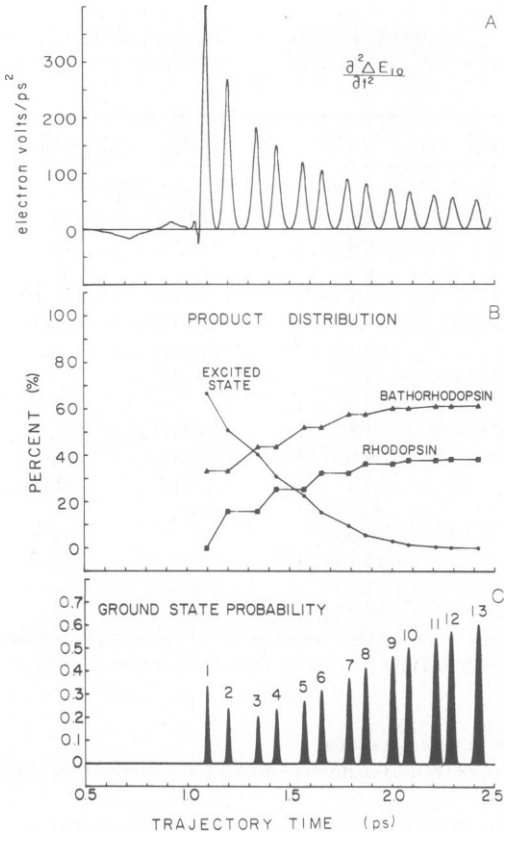

FIGURE 5

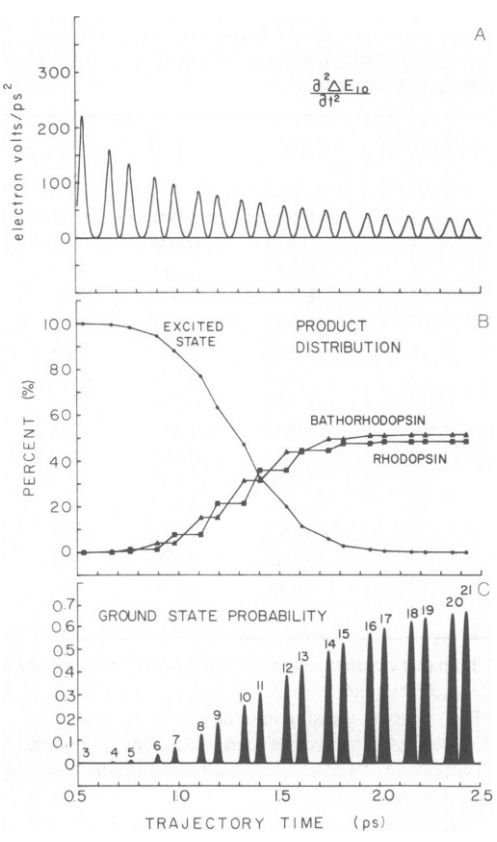

FIGURE 6

FIGURE 5 The second derivative of the potential energy difference between the ground and excited state with respect to time is plotted in *A* (see text). The ground-state product distribution *B*, and the probability of crossing into the ground state $a_0^2(\tau)$ *C*, plotted as a function of trajectory time for the photochemical isomerization of rhodopsin to bathorhodopsin (Table I, Fig. 3).

FIGURE 6 The second derivative of the potential energy difference between the ground and excited state with respect to time is plotted in *A* (see text). The ground-state product distribution (*B*), and the probability of crossing into the ground state $a_0^2(\tau)$ (*C*), plotted as a function of trajectory time for the photochemical isomerization of bathorhodopsin to rhodopsin (Table II, Fig. 4).

probability of crossing into the ground state. The sharpness of the probability function (a_0^2) at $\phi_{11,12} = 90°$ is primarily due to the high curvature of the excited-state potential well at the orthogonal dihedral angle.

A calculation of the quantum yield of rhodopsin photoisomerization proceeds as follows. The first trajectory following excitation enters the "activated complex" in ~1 ps and arrives at $\phi_{11,12} = 90°$ in 1.098 ps (Table I). The probability of crossing into the ground state during this first pass is 0.333, which means that ~33% of the molecules cross into the ground state to produce isomerized product in ~1.9 ps (Table I, row 1). The remaining 67% of the molecules continue on the excited-state trajectory which is now "trapped" in the activated complex in a low frequency (~150 cm^{-1}) torsional mode of the 11,12 dihedral angle. The second pass

through the 90° region occurs at 1.2 ps and the probability of crossing into the ground state is 0.238. Accordingly, ~24% of the remaining excited-state molecules undergo internal conversion to produce ~16% unisomerized product in ~1.6 ps (Table I, row 2). Torsional oscillations in the activated complex continue to pass through the 90° region transferring molecules to the ground state. After 14 torsional oscillations, >99.9% of the excited-state molecules have crossed into the ground state to produce 61.5% isomerized product (bathorhodopsin) and 38.5% unisomerized starting material (rhodopsin) (Table I, row 14). The above statistical analysis predicts a quantum yield of isomerization of 0.62 which is in reasonable agreement with the observed value of 0.67 (23). The fact that the calculations underestimate the quantum yield is probably associated with one or more of the following factors: (*a*) the model underestimates the torsional velocity of the isomerization; (*b*) the neglect of the nonadiabatic coupling function $\langle \psi_2 | \partial \psi_1 / \partial t \rangle$ in Eq. 4 underestimates the probability of crossing into the ground state (21); and/or (*c*) the excited-state potential surface is more asymmetric than predicted (Fig. 1) because our model of the binding site (Fig. 2) neglects important protein-chromophore interactions. In particular, our neglect of the second counterion which is predicted to be present in the binding site (32) and our underestimation of the bathorhodopsin relative energy (29) suggest the third factor is probably important. The fact that we have neglected many degrees of freedom in the chromophore potential surface suggests that the first factor may also be important. The extent to which neglect of the nonadiabatic coupling function is important will be discussed in more detail below.

Analysis of the quantum yield of bathorhodopsin photoisomerization is presented in Table II. Following excitation, the molecule reaches the activated complex in <0.3 ps due to the steep slope of the 11,12 torsional potential surface. (Our simplified potential surface neglects partitioning torsional relaxation into distortion of the 9,10 double bond, and therefore rhodopsin [11-*cis*] is the only photochemical product theoretically predicted [see below]). The molecule enters the activated complex with a considerable excess of vibrational energy (Fig. 4), and this excess energy prevents the first few trajectory passes through the 90° region from efficiently crossing into the ground state (ΔW is large). A total of 11 passes through the 90° dihedral angle are required before >63% of the excited-state molecules internally convert to the ground-state manifold to produce product in ~1.8 ps (Table II, row 11). After 18 passes 99.8% of the molecules are in the ground state, 48.4% in the 11-*cis* conformation (rhodopsin), and 51.4% in the original 11-*transoid* conformation (bathorhodopsin). The calculated quantum yield is therefore 0.48 in good agreement with the observed value of 0.5 (22).

The trajectory associated with the bathorhodopsin to rhodopsin transformation appears somewhat anomalous in that the first pass of the trajectory is trapped in the activated complex region even though it appears that the trajectory energy is significantly higher than the barrier height of the local potential well. The confusion is resolved by recognizing that the vertical axis represents the total energy of the chromophore-lysine system. The total energy is a sum of three components: $E_s(\phi)$, the energy of the torsional potential surface; $E_{kin}(\tau)$, the kinetic energy of the torsional motion; and $E_{vib}(\tau)$, the vibrational energy associated with the remaining modes of the polyene-lysine moiety. The reason the first and all subsequent trajectory elements are trapped in the activated complex is due to the fact that the kinetic energy of torsional motion is efficiently transferred to other "nonproductive" vibrational modes of the polyene-lysine system (see discussion concerning Eq. 1). Although the first

trajectory pass is a relatively high-velocity trajectory reaching a kinetic energy maximum of 0.23 eV (5.3 kcal/mol), "reflection" of the first trajectory at $\phi_{11,12} \simeq 75°$ back into the region of the activated complex occurs because the torsional kinetic energy is insufficient to override the local barrier associated with the activated complex potential well (see Fig. 7).

The reason the calculated quantum yield is closer to the experimental value for the bathorhodopsin → rhodopsin photoisomerization (error = 4%) than for the rhodopsin → bathorhodopsin photoisomerization (error = 8%) is probably due to the lack of sensitivity of the former calculation to errors in the excited state potential surface. The almost even distribution of 11-*cis* and 11-*transoid* isomers calculated for bathorhodopsin photoisomerization is due to the fact that the molecule enters the activated complex with a large excess of vibrational energy. The exact shape of the potential surface is not as important as the fact that it exhibits a large "downward" slope in the direction of the activated complex. The slope could be twice as large as that shown in Fig. 1 and the calculated quantum yield would be virtually identical to that predicted in Table II. In summary, therefore, the success of our calculation on bathorhodopsin suggests that our basic model is realistic but does not indicate that the potential surface shown in Fig. 1 is necessarily accurate.

Comparison with Other Models

Rosenfeld et al. (17) have suggested that the photochemical behavior of cattle rhodopsin is best rationalized in terms of a "common excited state" hypothesis (17). This hypothesis was based on the experimental observation that the quantum yields of rhodopsin and bathorhodopsin photoisomerization from the common excited-state activated complex appeared to sum to one within experimental error. The more recent experimental results of Suzuki and Callender

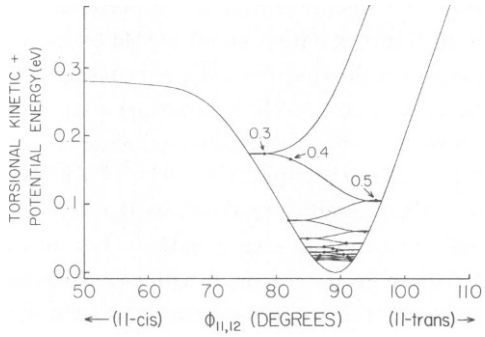

FIGURE 7 The total energy associated with the torsional degree of freedom as a function of dihedral angle ($\phi_{11,12}$) in the vicinity of the excited-state activated complex. The potential energy surface is plotted relative to $E_{S_1}(\phi_{11,12} = 90°)$ set equal to zero to facilitate superposition of the trajectory associated with the photochemical generation of the activated complex from excited bathorhodopsin. The excited-state trajectory is plotted with the vertical axis representing the excited state torsional kinetic plus potential energy and the energy associated with the other vibrational degrees of freedom of the polyene-lysine system is not included in the trajectory plot. The solid circles represent trajectory increments of 0.1 ps and trajectory times of 0.3, 0.4 and 0.5 ps after excitation are indicated. Note that the first trajectory pass through $\phi_{11,12} = 90°$ is trapped in the activated complex because the torsional kinetic energy is rapidly transfered to other vibrational degrees of freedom and the remaining kinetic energy is insufficient to override the small *"cisoid"* barrier [$\Delta E_r(\phi_{11,12} = 70°) - \Delta E_r(90°) \sim 0.24$ eV] associated with the activated complex.

(22), however, indicate that the quantum yields sum to more than one (see above). Consequently, the primary experimental evidence for a common equilibrated excited state no longer exists.

The calculations presented in this paper, and their relative success in predicting quantum yields, suggest that a one-dimensional torsional excited state potential surface is useful (though not rigorous) in simulating the photochemical interconversion of rhodopsin and bathorhodopsin. This one-dimensional torsional surface contains a potential well centered at $\phi_{11,12} = 90°$ which dynamically traps the trajectory during isomerization (Figs. 3 and 4) in an activated complex. The extent to which this activated complex represents the "common excited state" discussed by Rosenfeld et al. (17), is a question of semantics. However, our calculations indicate that the characteristics of the activated complex are strongly influenced by the vibrational energy and velocity of the entrance trajectory. Consequently, the supposition that the "common excited state" represents a fully equilibrated species trapped at $\phi_{11,12} = 90°$ is not supported by our calculations.

Warshel and Weiss (21) have presented an interesting analysis of the importance of the nonadiabatic coupling function in Eq. 3. Their calculations imply that the semiclassical treatment (Eq. 4) will underestimate the probability of crossing into the ground state because this coupling function is inherently neglected. Warshel and Weiss suggest that the probability of crossing into the ground state is ~0.5 on each pass through $\phi_{11,12} = 90°$. This value is significantly larger than the 0.333 value calculated by our formalism for the first pass in the photoisomerization of rhodopsin (Table I, row 1). A value of 0.5 on each pass will improve the calculated quantum yield from 0.62 (our value) to 0.67 (Warshel & Weiss [21]). However, complications are encountered in the application of Warshel and Weiss's theory to bathorhodopsin photoisomerization where the observed quantum yield is 0.5. One way to reconcile a first pass probability of 0.5 with a quantum yield of 0.5 is to assume the excited-state surface has more than one sharp potential well. While this is not impossible, the very steep $\phi_{11,12} = 90°$ to $\phi_{11,12} = 180°$ surface (Fig. 1) suggests to us that a second potential well in this region is unlikely.

Cattle Versus Squid Rhodopsin Binding Site Morphology

The photoisomerization of cattle bathorhodopsin is observed to strongly favor the formation of rhodopsin ($\phi_{t\to 11} = 0.5$) over isorhodopsin ($\phi_{t\to 9} = 0.054$) (22). In contrast, the photoisomerization of squid bathorhodopsin is observed to be relatively nonselective ($\phi_{t\to 11} = 0.36$, $\phi_{t\to 9} = 0.24$) (21). These data suggest that there are important differences in the binding sites of cattle and squid pigments.

The selectivity of cattle rhodopsin could be ascribed to an amino acid moiety within the binding site that is partially blocking 9-*trans* to 9-*cis* dihedral motion. This explanation, however, is unlikely given the rapid (~3 ps) photoisomerization time of the cattle isorhodopsin to bathorhodopsin reaction (16). A more likely possibility is that the opsin binding site prevents the 11,12 double bond of the chromophore from reaching planarity in bathorhodopsin. If the 11,12 (*trans*) dihedral angle were more distorted than the 9,10 (*trans*) dihedral angle, the formation of rhodopsin (11-*cis*) over isorhodopsin (9-*cis*) would be dynamically favored. Although our calculated potential surface predicts a significant nonplanarity of the equilibrium 11,12 dihedral angle in bathorhodopsin (Fig. 1), this prediction is due primarily to

our neglect of other degrees of freedom of the chromophore. Accordingly, our potential surface is probably overestimating the distortion of the 11,12 double bond in bathorhodopsin (see discussion in reference 11). Our calculations indicate, however, that an out-of-plane distortion of between 9 and 17° in the 11,12 *trans* double bond would be sufficient to dynamically favor the photochemical formation of rhodopsin over isorhodopsin by the order of magnitude observed for cattle bathorhodopsin. (The above calculation assumded a 5° out-of-plane distortion in the 9,10 dihedral angle [$\phi_{9,10} = 175°$]). In contrast, the observed quantum yields for squid bathorhodopsin photochemistry suggest the 9,10 and 11,12 dihedral angles in squid bathorhodopsin are distorted to roughly equal degrees of nonplanarity. This supposition follows from the observation of very similar *trans* to 9-*cis* and 11-*cis* quantum yields (see above).

The exact morphology of the binding site in cattle rhodopsin is not yet known. Accordingly, the environmental constraints responsible for inducing significant nonplanarity in the 11,12 double bond of the chromophore in bathorhodopsin cannot be specified with any certainty. Our simple model for the rhodopsin binding site predicts that a considerable fraction of the excess energy of bathorhodopsin relative to rhodopsin (calc = 26 kcal/mol [Fig. 1], obsvd = 35 kcal/mol [29]) is associated with compression of the lysine residue in bathorhodopsin. (Fig. 2) (see also reference 11). The chromophore will respond to the lysine "resistance" through dihedral distortion. As noted above, our calculations arbitrarily place all of the distortion into the 11,12 dihedral angle (Fig. 1), but a more realistic model would provide for energy minimization involving all of the degrees of freedom. INDO-CISD calculations indicate that the torsional relaxation will favor distortion of those double bonds closest to the protonated nitrogen whose resonance stabilization of the positive charge leads to a degree of bond order reversal.[2] Accordingly, compression of the lysine residue in bathorhodopsin is predicted to distort the 11,12 dihedral angle more than the 9,10 dihedral angle from planarity. The dynamic and conformational considerations, therefore, both lead to similar conclusions.

APPENDIX

One Dimensional Lagrangian Interpolation and Gradient Formulae

Our simulation of the molecular dynamics of the photoisomerization in rhodopsin and bathorhodopsin is based on the use of a classical one-dimensional Hamiltonian with the appropriate holonomic constraints (33) (see assumptions 2, 3 and 4 in section on Potential Surfaces of Isomerization). The torsional potential surfaces of the ground and excited states were obtained in a separate series of calculations using INDO-CISD molecular orbital theory (polyene portion) and force-field calculations (lysine residue) (11). These calculations provide values for $E^*(\phi)$ (excited state) and $E°(\phi)$ (ground state) at discrete values of ϕ, but the simulation of a dynamic process along a given potential surface requires

[2]The π-electron bond orders in the ground state of the all-*trans* protonated Schiff base of retinal are calculated for selected single bonds to be: P(8,9) = 0.3566, P(10,11) = 0.3870, P(12,13) = 0.4516, P(14,15) = 0.5573; and for selected double bonds: P(7,8) = 0.8557, P(9,10) = 0.8254, P(11,12) = 0.7933, P(13,14) = 0.7182, P(15,16) = 0.6276. The calculation was performed using INDO-CISD molecular orbital procedures including 127 single and 353 double excitations in the CI Hamiltonian (11). A standard geometry was assumed as described in (11). Note that the bond order for the 9,10 double bond (0.8254) is larger than the bond order for the 11,12 double bond (0.7933). This observation suggests that the π-electron system can sustain larger out-of-plane distortion of the 11,12 double bond than the 9,10 double bond, an observation which has been confirmed by energy-minimization calculations.

accurate interpolation between these discrete values. The following set of algorithms provide accurate and computationally efficient interpolative, gradient and higher derivative values along the potential surface. For the purposes of generality, the formulae are presented in terms of a one-dimensional cartesian coordinate, x. Appropriate transformations can be applied to express any one-dimensional problem in terms of a pseudo-linearilized coordinate (33).

Assume, for the purposes of generality, that the system in question is currently at position x on the potential surface. Let the local region of the potential surface be defined by the discrete energies $E_1(x_1)$, $E_2(x_2)$, $E_3(x_3)$, $E_4(x_4)$ and $E_5(x_5)$ where $x_3 > x \gg x_4$. The following analytical formulae based on five-point Lagrangian interpolation algorithms (34) provide values for $E(x)$, $\Delta E(x)/\Delta x$ and $\Delta^2 E(x)/\Delta x^2$. Define:

$$d_1 = [(x_1 - x_2)(x_1 - x_3)(x_1 - x_4)(x_1 - x_5)]^{-1}, \tag{A1}$$

$$d_2 = [(x_2 - x_1)(x_2 - x_3)(x_2 - x_4)(x_2 - x_5)]^{-1}, \tag{A2}$$

$$d_3 = [(x_3 - x_1)(x_3 - x_2)(x_3 - x_4)(x_3 - x_5)]^{-1}, \tag{A3}$$

$$d_4 = [(x_4 - x_1)(x_4 - x_2)(x_4 - x_3)(x_4 - x_5)]^{-1}, \tag{A4}$$

$$d_5 = [(x_5 - x_1)(x_5 - x_2)(x_5 - x_3)(x_5 - x_4)]^{-1}, \tag{A5}$$

Then $E(x)$ is given by

$$\begin{aligned} E(x) = {} & E_1 d_1 (x - x_2)(x - x_3)(x - x_4)(x - x_5) \\ & + E_2 d_2 (x - x_1)(x - x_3)(x - x_4)(x - x_5) \\ & + E_3 d_3 (x - x_1)(x - x_2)(x - x_4)(x - x_5) \\ & + E_4 d_4 (x - x_1)(x - x_2)(x - x_3)(x - x_5) \\ & + E_5 d_5 (x - x_1)(x - x_2)(x - x_3)(x - x_4). \end{aligned} \tag{A6}$$

The first derivative of the potential energy with respect to coordinate, $\Delta E(x)/\Delta x$, is given by the following set of equations. Define:

$$\begin{aligned} a_1 = {} & r - s(x_2 + x_3 + x_4 + x_5) \\ & + t(x_2x_3 + x_2x_4 + x_2x_5 + x_3x_4 + x_3x_5 + x_4x_5), \end{aligned} \tag{A7}$$

$$\begin{aligned} a_2 = {} & r - s(x_1 + x_3 + x_4 + x_5) \\ & + t(x_1x_3 + x_1x_4 + x_1x_5 + x_3x_4 + x_3x_5 + x_4x_5), \end{aligned} \tag{A8}$$

$$\begin{aligned} a_3 = {} & r - s(x_1 + x_2 + x_4 + x_5) \\ & + t(x_1x_2 + x_1x_4 + x_1x_5 + x_2x_4 + x_2x_5 + x_4x_5), \end{aligned} \tag{A9}$$

$$\begin{aligned} a_4 = {} & r - s(x_1 + x_2 + x_3 + x_5) \\ & + t(x_1x_2 + x_1x_3 + x_1x_5 + x_2x_3 + x_2x_5 + x_3x_5), \end{aligned} \tag{A10}$$

$$\begin{aligned} a_5 = {} & r - s(x_1 + x_2 + x_3 + x_4) \\ & + t(x_1x_2 + x_1x_3 + x_1x_4 + x_2x_3 + x_2x_4 + x_3x_4), \end{aligned} \tag{A11}$$

where

$$r = 4x^3, \tag{A12}$$

$$s = 3x^2, \tag{A13}$$

and

$$t = 2x, \tag{A14}$$

then:

$$\begin{aligned}\Delta E(x)/\Delta x = {} & E_1 d_1 (a_1 - x_2x_3x_4 - x_2x_3x_5 - x_2x_4x_5 - x_3x_4x_5) \\ & + E_2 d_2 (a_2 - x_1x_3x_4 - x_1x_3x_5 - x_1x_4x_5 - x_3x_4x_5) \\ & + E_3 d_3 (a_3 - x_1x_2x_4 - x_1x_2x_5 - x_1x_4x_5 - x_2x_4x_5) \\ & + E_4 d_4 (a_4 - x_1x_2x_3 - x_1x_2x_5 - x_1x_3x_5 - x_2x_3x_5) \\ & + E_5 d_5 (a_5 - x_1x_2x_3 - x_1x_2x_4 - x_1x_3x_4 - x_2x_3x_4).\end{aligned} \tag{A15}$$

The second derivative of the potential energy with respect to coordinate, $\Delta^2 E(x)/\Delta x^2$, is calculated by redefining the r, s, and t variables that appear in Eqs. A7–A11;

$$r = 12x^2 \tag{A16}$$

$$s = 6x, \tag{A17}$$

$$t = 2, \tag{A18}$$

and evaluating the following expression:

$$\Delta^2 E(x)/\Delta x^2 = E_1 d_1 a_1 + E_2 d_2 a_2 + E_3 d_3 a_3 + E_4 d_4 a_4 + E_5 d_5 a_5. \tag{A19}$$

Newton's equations of motion can be solved by recognizing that the force acting on the center of mass of the system is simply $-\Delta E(x)/\Delta x$. Accordingly, the acceleration of the center of mass, $a(x)$, is given by:

$$a(x) = -(\Delta E(x)/\Delta x)/M \tag{A20}$$

where M is the total mass of the system of particles. The velocity, $v(\tau)$, of the center of mass at trajectory time τ is "updated" using the following algorithm,

$$v(\tau) = a(x)\,\delta t + v(\tau - \delta t) - \text{sign}\,[v(\tau - \delta t)][2(\Delta E_{\text{kin}}/\Delta t)\,\delta t/M]^{1/2} \tag{A21}$$

where δt is the trajectory increment, the "sign" function returns the sign of the velocity (± 1), and $\Delta E_{\text{kin}}/\Delta t$ is calculated using Eq. 1. The energy difference between the excited and ground state surfaces, $\Delta E_{10}(x) = E^*(x) - E^\circ(x)$, can be calculated by substituting the appropriate energy separations at positions $x_1 \ldots x_5$ for the values $E_1 \ldots E_5$ in Eq. A6. Furthermore, the second derivative of energy separation with respect to time can be calculated to good precision using the relationship:

$$(\partial^2 \Delta E_{10}/\partial t^2)_{t=\tau} \simeq [v(\tau)]^2\,\{\Delta^2[\Delta E_{10}(x)]/\Delta x^2\} \tag{A22}$$

where the second derivative $[\Delta^2[\Delta E_{10}(x)]/\Delta x^2]$ is evaluated using:

$$\begin{aligned}\Delta^2[\Delta E_{10}(x)]/\Delta x^2 = {} & (E_1^* - E_1^\circ)\,d_1 a_1 + (E_2^* - E_2^\circ)\,d_2 a_2 \\ & + (E_3^* - E_3^\circ)\,d_3 a_3 + (E_4^* - E_4^\circ)\,d_4 a_4 + (E_5^* - E_5^\circ)\,d_5 a_5\end{aligned} \tag{A23}$$

where $a_1 \ldots a_5$ and $d_1 \ldots d_5$ are defined as in Eq. A19.

This work was supported in part by grants from the National Institutes of Health, the National Council to Combat Blindness (Fight for Sight, Inc., New York) and the National Science Foundation.

The authors are grateful to R. H. Callender, A. Cooper, B. Honig, D. S. Kliger, R. Mathies, A. Warshel, and R. M. Weiss for interesting and helpful discussions.

Received for publication 29 July 1980 and in revised form 28 January 1981.

REFERENCES

1. Yoshizawa, T., and G. Wald. 1963. Pre-lumirhodopsin and the bleaching of visual pigments. *Nature (Lond.).* 197:1279–1286.
2. Birge, R. R. 1981. Photophysics of light transduction in rhodopsin and bacteriorhodopsin. *Annu. Rev. Biophys. Bioeng.* 10:315–54.
3. Busch, G., M. Applebury, A. Lamola, and P. Rentzepis. 1972. Formation and decay of prelumirhodopsin at room temperature. *Proc. Natl. Acad. Sci. U.S.A.* 69:2802–2806.
4. Applebury, M. L., K. Peters, and P. Rentzepis. 1978. Primary intermediates in the photochemical cycle of bacteriorhodopsin. *Biophys. J.* 23:375–382.
5. Peters, K., M. Applebury, and P. Rentzepis. 1977. Primary photochemical event in vision: proton translocation. *Proc. Natl. Acad. Sci. U.S.A.* 74:3119–3123.
6. van der Meer, K., J. J. C. Mulder, and J. Lugtenberg. 1976. A new facet in rhodopsin photochemistry. *Photochem. Photobiol.* 24:363–367.
7. Lewis, A. 1978. The molecular mechanism of excitation in visual transduction and bacteriorhodopsin. *Proc. Natl. Acad. Sci. U.S.A.* 75:549–553.
8. Favrot, J., S. M. Leclercq, R. Roberge, C. Sandorfy, and D. Vocelle. 1979. Intramolecular interactions in visual pigments. The hydrogen bond in vision. *Photochem. Photobiol.* 29:99–108.
9. Huppert, D., P. M. Rentzepis, and D. S. Kliger. 1977. Picosecond and nanosecond isomerization kinetics of protonated 11-*cis* retinylidene schiff bases. *Photochem. Photobiol.* 25:193–197.
10. Warshel, A. 1976. Bicycle-pedal model for the first step in the vision process. *Nature (Lond.).* 260:679–683.
11. Birge, R. R., and L. M. Hubbard. 1980. Molecular dynamics of *cis-trans* isomerization in rhodopsin. *J. Am. Chem. Soc.* 102:2195–2205.
12. Eyring, G., B. Curry, R. Mathies, R. Fransen, I. Palings, and J. Lugtenburg. 1980. Interpretation of the resonance raman spectrum of bathorhodopsin based on visual pigment analogues. *Biochemistry.* 19:2410–2418.
13. Akita, H., S. P. Tanis, M. Adams, V. Balogh-Nair, and K. Nakanishi. 1980. Non-bleachable rhodopsins retaining the full natural chromophore. *J. Am. Chem. Soc.* 102:6370–6372.
14. Doukas, A. G., B. Aton, R. H. Callender, and T. G. Ebrey. 1978. Resonance raman studies of bovine metarhodopsin I and metarhodopsin II. *Biochemistry.* 17:2430–2435.
15. Honig, B., T. G. Ebrey, R. H. Callender, U. Dinur, and M. Ottolenghi. 1979. Photoisomerization, energy storage, and charge separation: a model for light energy transduction in visual pigments and bacteriorhodopsin. *Proc. Natl. Acad. Sci. U.S.A.* 76:2503–2507.
16. Green, B., T. Monger, R. Alfano, B. Aton, and R. Callender. 1977. *Cis-trans* isomerization in rhodopsin occurs in picoseconds. *Nature (Lond.).* 269:179–180.
17. Rosenfeld, T., B. Honig, M. Ottolenghi, J. Hurley, and T. G. Ebrey. 1977. *Cis-trans* isomerization in the photochemistry of vision. *Pure Appl. Chem.* 49:341–351.
18. Honig, B., A. Greenberg, U. Dinur, and T. G. Ebrey. 1976. Visual-pigment spectra: implications of the protonation of the retinal schiff base. *Biochemistry.* 14:4593–4599.
19. Honig, B., and T. G. Ebrey. 1976. The storage of light energy in the batho-product of rhodopsin. *Biophys. J.* 16:98*a*.
20. Ottolenghi, M. 1980. The photochemistry of rhodopsin. *Adv. Photochem.* 12:97–200.
21. Warshel, A., and R. M. Weiss. 1979. A new view of the dynamics of singlet *cis-trans* photoisomerization. *J. Am. Chem. Soc.* 101:6131–6133.
22. Suzuki, T., and R. H. Callender. 1981. Primary photochemistry and photoisomerization of retinal at 77 K in cattle and squid rhodopsin. *Biophys. J.* 34:261–270.
23. Dartnall, H. J. A. 1972. Photosensitivity. *In* Handbook of Sensory Physiology, vol. VII/1:122–145.
24. Birge, R. R., K. Schulten, and M. Karplus. 1975. Possible influence of a low-lying "covalent" excited state on the absorption spectrum and photoisomerization of 11-*cis* retinal. *Chem. Phys. Lett.* 31:451–455.

25. Birge, R. R., J. A. Bennett, B. M. Pierce, and T. M. Thomas. 1978. Two-photon spectroscopy of the visual chromophores. Evidence for a lowest excited $^1A_g^-$-like $\pi\pi^*$ state in all-*trans*-retinol (vitamin A). *J. Am. Chem. Soc.* 100:1533–1539.
26. Birge, R. R., and B. M. Pierce. 1979. A theoretical analysis of the two-photon properties of linear polyenes and the visual chromophores. *J. Chem. Phys.* 70:165–178.
27. Birge, R. R., C. T. Berge, L. L. Noble, and R. C. Neuman. 1979. Effect of external pressure on the spectroscopic and conformational properties of the visual chromophores. *J. Am. Chem. Soc.* 101:5162–5170.
28. Blatchly, R. A., J. D. Carriker, V. Balogh-Nair, and K. Nakanishi. 1980. Adamantyl allenic rhodopsin. Leniency of the ring binding site in bovine opsin. *J. Am. Chem. Soc.* 102:2495–2497.
29. Cooper, A. 1979. Energy uptake in the first step of visual excitation. *Nature (Lond.).* 282:531–533.
30. Warshel, A., and M. Karplus. 1975. Semiclassical trajectory approach to photoisomerization. *Chem. Phys. Lett.* 32:11–17.
31. Miller, W. H., and T. F. George. 1972. Semiclassical theory of electronic transitions in low energy atomic and molecular collisions involving several nuclear degrees of freedom. *J. Chem. Phys.* 56:5637–5652.
32. Honig, B., V. Dinur, K. Nakanishi, V. Balogh-Nair, M. A. Gawinowicz, M. Arnaboldi, and M. G. Motto. 1979. An external point-charge model for wavelength regulation in visual pigments. *J. Am. Chem. Soc.* 101:7084–7086.
33. Goldstein, H. 1980. Classical mechanics, second edition. Addison-Wesley, Reading, Mass. Chapters 1–5, 8–10.
34. Southworth, R. W., and S. L. Deleeuw. 1965. Digital Computation and Numerical Methods. McGraw-Hill, Inc., New York, 313–317, 323.